REPORT SSD-TR-90-29

AEROSPACE REPORT NO.
TR-0089(4930-06)-3

AD-A230 183

Degenerate Four-Wave Mixing of CW HF Laser Bear s in HF Absorption Cell

Prepared by

H. MIRELS, J. G. COFFER, J. M. BERNARD, and R. A. CHODZKO
Aerophysics Laboratory
Laboratory Operations

DTIC
ELECTE
DEC 20 1990
S D
D

6 August 1990

Prepared for

SPACE SYSTEMS DIVISION
AIR FORCE SYSTEMS COMMAND
Los Angeles Air Force Base
P.O. Box 92960
Los Angeles, CA 90009-2960

Development Group

THE AEROSPACE CORPORATION
El Segundo, California

APPROVED FOR PUBLIC RELEASE;
DISTRIBUTION UNLIMITED

90

This report was submitted by The Aerospace Corporation, El Segundo, CA 90245-4691, under Contract No. F04701-88-C-0089 with the Space Systems Division, P. O. Box 92960, Los Angeles, CA 90009-2960. It was reviewed and approved for The Aerospace Corporation by R. W. Fillers, Director, Aerophysics Laboratory. Captain Rafael Riviere was the Air Force project officer for the Mission-Oriented Investigation and Experimentation (MOIE) program.

This report has been reviewed by the Public Affairs Office (PAS) and is releasable to the National Technical Information Service (NTIS). At NTIS, it will be available to the general public, including foreign nationals.

This technical report has been reviewed and is approved for publication. Publication of this report does not constitute Air Force approval of the report's findings or conclusions. It is published only for the exchange and stimulation of ideas.

Rafael Riviere

RAFAEL RIVIERE, CAPT, USAF
MOIE Project Officer
SSD/CNL

Jonathan M. Emmes

JONATHAN M. EMMES, MAJ, USAF
MOIE Program Manager
AFSTC/WCO OL-AB

UNCLASSIFIED

SECURITY CLASSIFICATION OF THIS PAGE

REPORT DOCUMENTATION PAGE

1a. REPORT SECURITY CLASSIFICATION: Unclassified	1b. RESTRICTIVE MARKINGS
2a. SECURITY CLASSIFICATION AUTHORITY	3. DISTRIBUTION/AVAILABILITY OF REPORT: Approved for public release; distribution is unlimited.
2b. DECLASSIFICATION/DOWNGRADING SCHEDULE	
4. PERFORMING ORGANIZATION REPORT NUMBER(S): TR-0089(4930-06)-3	5. MONITORING ORGANIZATION REPORT NUMBER(S): SSD-TR-90-29
6a. NAME OF PERFORMING ORGANIZATION: The Aerospace Corporation Laboratory Operations; 6b. OFFICE SYMBOL (If applicable)	7a. NAME OF MONITORING ORGANIZATION: Space Systems Division
6c. ADDRESS (City, State, and ZIP Code): El Segundo, CA 90245-4691	7b. ADDRESS (City, State, and ZIP Code): Los Angeles, Air Force Base, Los Angeles, CA 90009-2960
8a. NAME OF FUNDING/SPONSORING ORGANIZATION; 8b. OFFICE SYMBOL (If applicable)	9. PROCUREMENT INSTRUMENT IDENTIFICATION NUMBER: F04701-88-C-0089
8c. ADDRESS (City, State, and ZIP Code)	10. SOURCE OF FUNDING NUMBERS: PROGRAM ELEMENT NO. / PROJECT NO. / TASK NO. / WORK UNIT ACCESSION NO.

11. TITLE (Include Security Classification)

DEGENERATE FOUR-WAVE MIXING OF CW HF LASER BEAMS IN HF ABSORPTION CELL

12. PERSONAL AUTHOR(S) Mirels, Harold; Coffer, John G.; Bernard, Jay M.; and Chodzko, Richard A.

13a. TYPE OF REPORT	13b. TIME COVERED	14. DATE OF REPORT (Year, Month, Day)	15. PAGE COUNT
	FROM ____ TO ____	1990 August 6	47

16. SUPPLEMENTARY NOTATION

17. COSATI CODES			18. SUBJECT TERMS (Continue on reverse if necessary and identify by block number)
FIELD	GROUP	SUB-GROUP	cw hydrogen fluoride laser, Degenerate four-wave mixing, Nonlinear optics, Phase conjugation

19. ABSTRACT (Continue on reverse if necessary and identify by block number)

Phase conjugation of a cw hydrogen fluoride (HF) laser beam has been investigated experimentally and theoretically using resonant degenerate four-wave mixing (DFWM) in an HF gas absorption cell. A single-line single-mode HF laser, operating on $P_1(8)$, $P_1(9)$, or $P_1(10)$ transitions, provided total (forward plus backward) pump beam intensities of 130, 600, and 400 W/cm^2, respectively, in the HF absorption cell. A probe beam intensity of the order of 10 W/cm^2 was also provided. Conjugate reflection of the probe beam was investigated as a function of gas cell pressure and as a function of frequency detuning from line center. The variation of reflectivity with gas cell pressure at fixed laser beam intensity indicated a peak reflectivity of the order of 10^{-4} at pressures from 2 to 4 Torr. Measurement of conjugate beam intensity, as a function of frequency detuning from line center, provided a signal with a full width at half maximum (FWHM) of about 30 MHz. The latter is of the order of the homogeneous width, for HF at the test pressure, and may be compared to the Doppler width $\Delta\nu_d$ = 300 MHz for the medium. An analytical model is presented which provides theoretical estimates for the variation of reflectivity with pressure. Effects of diffusion, thermal conduction, pump depletion, and a nonuniform (Gaussian) profile are considered. Theoretical estimates for peak reflectivity agree with experiments to within a factor of about 2.

20. DISTRIBUTION/AVAILABILITY OF ABSTRACT: [X] UNCLASSIFIED/UNLIMITED [ ] SAME AS RPT [ ] DTIC USERS	21. ABSTRACT SECURITY CLASSIFICATION: Unclassified
22a. NAME OF RESPONSIBLE INDIVIDUAL	22b. TELEPHONE (Include Area Code); 22c. OFFICE SYMBOL

DD FORM 1473, 84 MAR — 83 APR edition may be used until exhausted. All other editions are obsolete.

SECURITY CLASSIFICATION OF THIS PAGE

UNCLASSIFIED

CONTENTS

DTIC COPY INSPECTED 6

NTIS CRA&I
DTIC TAB
Unannounced
Justification

By

A-1 Special

FIGURES

TABLES

I. INTRODUCTION

Phase conjugation of a cw HF chemical laser beam is of interest for aberration correction in systems that employ these lasers. Studies of phase conjugation of an HF chemical laser beam by means of stimulated Brillouin scattering (SBS) are reported in Refs. 1 and 2. A difficulty with the SBS approach to HF laser phase conjugation is the need for megawatt power levels in order to achieve threshold.[3] In addition, the frequency of the conjugate beam is Doppler shifted from the incident beam. These limitations can be circumvented by employing degenerate four-wave mixing (DFWM) (e.g., Refs. 4-7). A theoretical study of the application of DFWM for phase conjugation of a pulsed, multiline HF chemical laser by use of a homogeneously broadened saturable gain medium is reported in Ref. 8.

The use of DFWM for phase conjugation of a cw HF chemical laser beam is investigated analytically and experimentally in this report. Analytic expressions are deduced for DFWM reflection coefficients associated with a saturable absorber. Effects of diffusion, heat conduction, pump depletion, and a Gaussian profile are considered. The experimental study employs a single-line, single-longitudinal mode cw HF laser operating at 1-10 W and a gaseous HF absorption cell operating at nominal pressures of 1-10 Torr. Experimental values of reflection coefficient are reported as a function of frequency detuning from line center and absorption cell pressure.

Symbols are defined in Appendix A. Spectroscopic and chemical rate data for HF are given in Appendix B.

II. THEORY

The DFWM process is illustrated in Fig. 1. Here, I_f, I_b, I_p, and I_c denote the intensity of the forward pump, backward pump, probe, and conjugate waves, respectively. The waves are assumed to have the same frequency and to interact in a saturable medium. The forward and backward pump waves are required to be phase conjugates. This is easily achieved by the use of counter-propagating plane waves from a single laser source. The angle between I_p and I_f is denoted θ and is assumed small in this study.

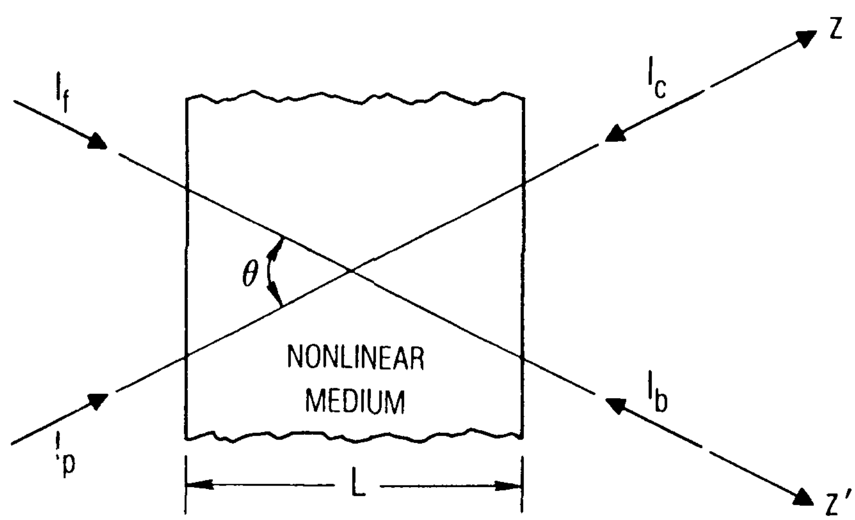

Fig. 1. Geometry for DFWM.

The physical basis for the generation of I_c is illustrated in Fig. 2. The interaction between waves I_p and I_f creates a stationary sinusoidal interference pattern of wavelength $\lambda_{pf} = \lambda/[2 \sin(\theta/2)]$ which interacts with the saturable medium to form a sinusoidal variation in medium susceptibility. The latter scatters the incident beam I_b to form I_c, which can be shown to be the phase conjugate of I_p. Similarly, I_p and I_b form a grating of wavelength $\lambda_{pb} = \lambda/[2 \cos(\theta/2)]$ which scatters I_f to add

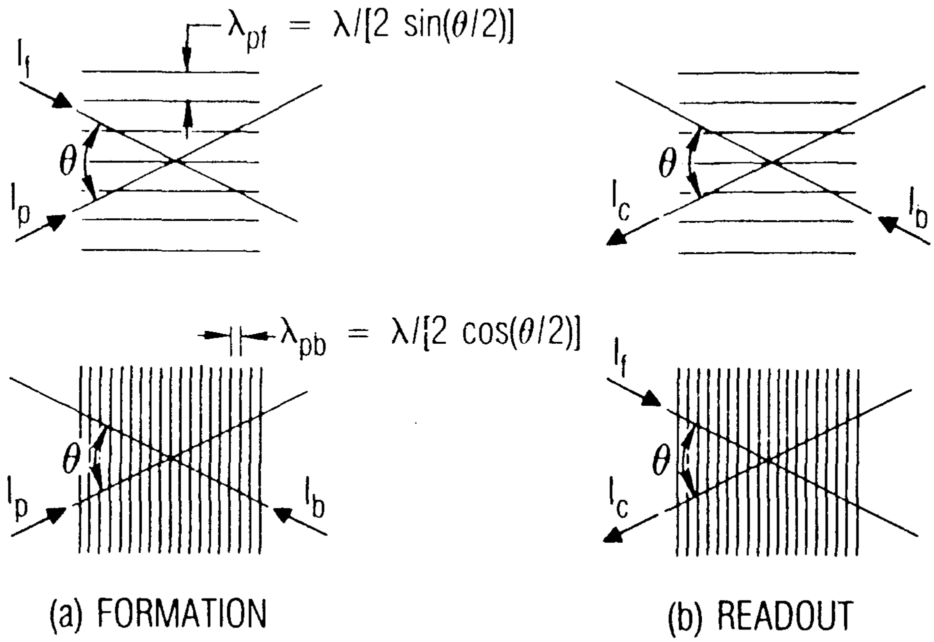

Fig. 2. Grating Formation and Readout in DFWM.

coherently to the phase conjugate I_c. For small θ, the gratings λ_{pf} and λ_{pb} are termed "wide" and "narrow," respectively.

In the following sections, we summarize expressions for the reflectivity $R \equiv I_c/I_p$ for both homogeneously and inhomogeneously broadened saturable media. To simplify the expressions, we assume $I_f = I_b$, $I_{p,c} << I_{f,b}$, and $\theta^2 << 1$. Beam intensity is assumed to be uniform in the transverse direction. The effects of a Gaussian intensity profile, diffusion, heat conduction, and pump depletion are also considered.

A. HOMOGENEOUS MEDIUM

Reflectivity expressions for a homogeneously broadened saturable medium, in the limit $I_{p,c} << I_{f,b}$ and $\theta^2 << 1$, are given in Appendix C. When pump depletion effects are negligible and $I_f = I_b$, the reflectivity is, from Eq. (C-9b),

$$(1 + \delta^2) \frac{R}{(\alpha_0^E L)^2} = \frac{(I_t/I_s)^2 \, [1 + O(\alpha_0^E L)]}{[1 + 2(I_t/I_s)]^3} \tag{1}$$

where a term of order $\alpha_0^E L$ is neglected and

$$I_t = I_f + I_b \tag{2a}$$

$$I_s = I_s^0 (1 + \delta^2) \tag{2b}$$

$$\delta = (\nu - \nu_0)/(\Delta\nu_h/2) \tag{2c}$$

Here, I_s^0 is a suitable line center ($\delta = 0$) saturation intensity, $\Delta\nu_h$ is the homogeneous width, L is the length over which the four waves interact, and α_0^E is the line center small-signal electric-field absorption coefficient. Expressions for I_s^0, α_0^E, and $\Delta\nu_h$ are given in Appendix B. The variation of $(1 + \delta^2)R/(\alpha_0^E L)^2$ with I_t/I_s is indicated in Fig. 3. The reflectivity has a maximum value given by

$$27(1 + \delta^2) \frac{R_{m,I}}{(\alpha_0^E L)^2} = 1 \tag{3}$$

which occurs at an intensity

$$I_t/I_s = 1 \tag{4}$$

The variation of $R/(\alpha_0^E L)^2$ with the detuning parameter δ, for fixed I_t/I_s^0, is indicated in Fig. 4. For each curve, the intensity is a maximum at $\delta = 0$. The half width at half maximum (HWHM) of these curves equals 0.51 in the limit $I_t/I_s^0 \to 0$ and increases with increase in I_t/I_s^0.

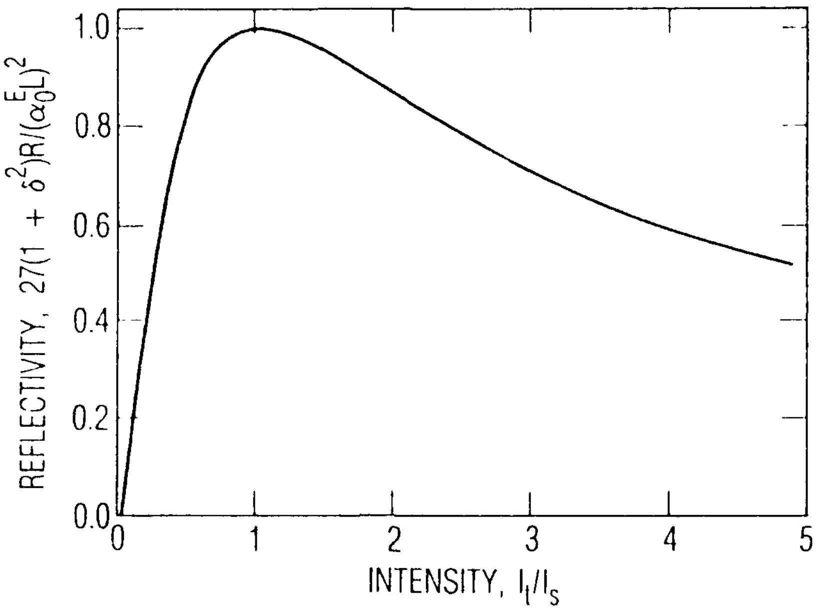

Fig. 3. Variation of Reflectivity with Intensity. Eq. (1), $\alpha_0^E L \ll 1$.

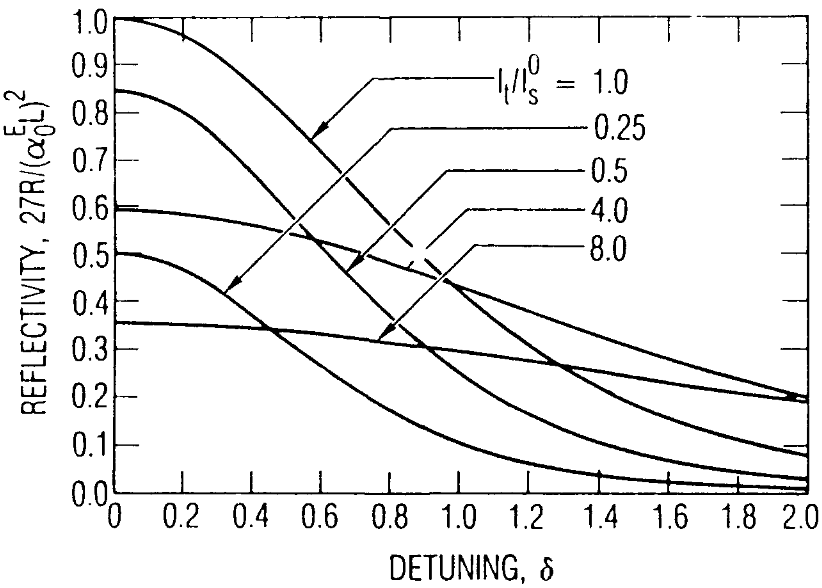

Fig. 4. Variation of Reflectivity with Detuning δ at Fixed I_t/I_s^0. $\alpha_0^E \ll 1$.

B. INHOMOGENEOUS MEDIUM

The analysis of degenerate four-wave mixing in an inhomogeneously broadened medium is complicated by the need to consider particle thermal velocity distributions. It is expected that only particles with velocity near zero (i.e., within the homogeneous width about line center) will be resonant with all four waves, thereby contributing to the interaction. It is also expected that the interaction will be similar to that for a homogeneously broadened medium with a like number of resonant particles. It has therefore been suggested[4] that the reflectivity R in an inhomogeneously broadened medium be computed from expressions deduced for a homogeneously broadened medium using appropriate inhomogeneous medium values for α_0^E and I_s. However, the effect of particle diffusion on reflectivity must be considered. The latter is evaluated in Appendix D.

Let R_D and R denote estimates for reflectivity which include and exclude, respectively, the effect of diffusion. The results of Appendix D indicate

$$\frac{R_D}{R} = \left(\frac{1/2}{1 + \tau D k_{pf}^2} + \frac{1/2}{1 + \tau D k_{pb}^2}\right)^2 \tag{5}$$

where the terms involving k_{pf} and k_{pb} represent the contributions of the wide and narrow gratings, respectively. For an inhomogeneously broadened medium (i.e., $\Delta\nu_h/\Delta\nu_d \ll 1$) and $\theta^2 \ll 1$, Eq. (5) becomes

$$\frac{R_D}{R} = \left(\frac{1/2}{1 + \tau D k_{pf}^2}\right)^2 [1 + \mathbf{0}(\theta^2)] \tag{6a}$$

In this limit, the narrow grating is washed out. The wide grating is fully effective when $\tau D k_{pf}^2 \ll 1$. In this limit $R_D/R = 1/4$. For an inhomogeneously broadened medium, $\theta^2 \ll 1$ and $\alpha_0^E L \ll 1$, Eqs. (1) and (6a) indicate

$$\frac{R_D}{(\alpha_0^E L)^2} = \frac{(I_t/I_s)^2[1 + \mathbf{0}(\alpha_0^E L)]}{[1 + 2(I_t/I_s)]^3} \left(\frac{1/2}{1 + \tau D k_{pf}^2}\right)^2 \tag{6b}$$

Equation (6b) is applicable to the present experimental study.

C. PRESSURE VARIATION EFFECT IN LIMIT $\delta^2 << 1$

The variation of reflectivity with cell pressure is of interest. We assume $\delta^2 << 1$. For the present case of a hydrogen fluoride gas at pressures of order 1-10 Torr, the pressure dependence of α_0^E and I_s^0 can be expressed as

$$\alpha_0^E = k_\alpha p \tag{7a}$$

$$I_s^0 = \kappa_s p^2 \tag{7b}$$

where p denotes cell pressure. Theoretical estimates for k_α and k_s are deduced in Appendix B and are listed in Table 1. We write I_s^0/I_t and $\alpha_0^E L$ in the form

$$I_s^0/I_t = 4(p/c_1)^2 \tag{8a}$$

$$\alpha_0^E L = c(p/c_1) \tag{8b}$$

where

$$c_1 = 2(I_t/\kappa_s)^{1/2} \tag{8c}$$

$$c = k_\alpha L c_1 \tag{8d}$$

Substitution into Eq. (6b) yields, for $\delta^2 << 1$,

$$\frac{216 R_D}{c^2} = \frac{27(p/c_1)^8 \, [1 + \mathbf{O}(c)]}{[2(p/c_1)^2 + 1]^3 \, [(p/c_1)^2 + B]^2} \tag{9a}$$

where B is independent of pressure and is given by

$$B = p^2 \tau D \, k_{pf}^2/c_1{}^2 \tag{9b}$$

Table 1. Absorption Coefficient and Saturation Intensity for HF $P_1(J)$ Transitions. $k_\alpha = \alpha_0^E/p$, $k_s = I_s^0/p^2$.

T (K)	J	k_α $\left(\frac{1}{\text{cm-Torr}}\right)$	k_s $\left(\frac{W}{(\text{cm-Torr})^2}\right)$
300	7	0.07943	78.52
300	8	0.01897	74.60
300	9	0.00364	71.14
300	10	0.00056	68.03
400	7	0.15808	52.49
400	8	0.05643	49.87
400	9	0.01702	47.55
400	10	0.00436	45.47
500	7	0.21055	38.40
500	8	0.09567	36.49
500	9	0.03786	34.79
500	10	0.01310	33.27
600	7	0.23437	29.75
600	8	0.12508	28.27
600	9	0.05932	26.96
600	10	0.02509	25.78

Equation (9a) provides the variation of R_D with pressure and is plotted in Fig. 5a. The reflectivity R_D has a maximum at

$$\left(\frac{p_m}{c_1}\right)^2 = (1/2)[1 + B + (1 + 10B + B^2)^{1/2}] \tag{10a}$$

which, for small and large B, becomes, respectively,

$$(p_m/c_1)^2 = 1 + 3B - 6B^2 + \mathbf{O}(B^3) \tag{10b}$$

$$= B[1 + (3/B) + \mathbf{O}(1/B^2)] \tag{10c}$$

The reflectivity maximum is denoted $(R_D)_{m,p}$ and is obtained by substitution of Eq. (10) into Eq. (9). For small and large B,

$$\frac{216(R_D)_{m,p}}{c^2} = 1 - 2B + \mathbf{O}(B^2) \tag{11a}$$

$$= \frac{27}{32B}\left[1 - \frac{3}{2B} + \mathbf{O}\left(\frac{1}{B^2}\right)\right] \tag{11b}$$

Equations (8a) and (10b) indicate that at the maximum point, $I_t/I_s^0 = (1/4)[1 + \mathbf{O}(B)]$. This result differs from Eq. (3b) due to the variation of α_0^E with p.

Corresponding values of B, p_m/c_1, $(R_D)_{m,p}/c^2$ and $(\tau D k_{pf}^2)_m = B/(p_m/c_1)^2$ are given in Table 2. These permit theoretical estimates of p_m and $(R_D)_{m,p}$ for given values of I_t, k_α, k_s, and L. Conversely, c, c_1, k_α and k_s can be deduced from experimental observation of p_m and $(R_D)_{m,p}$ for given I_t and L. The procedure is most accurate when $B \ll 1$.

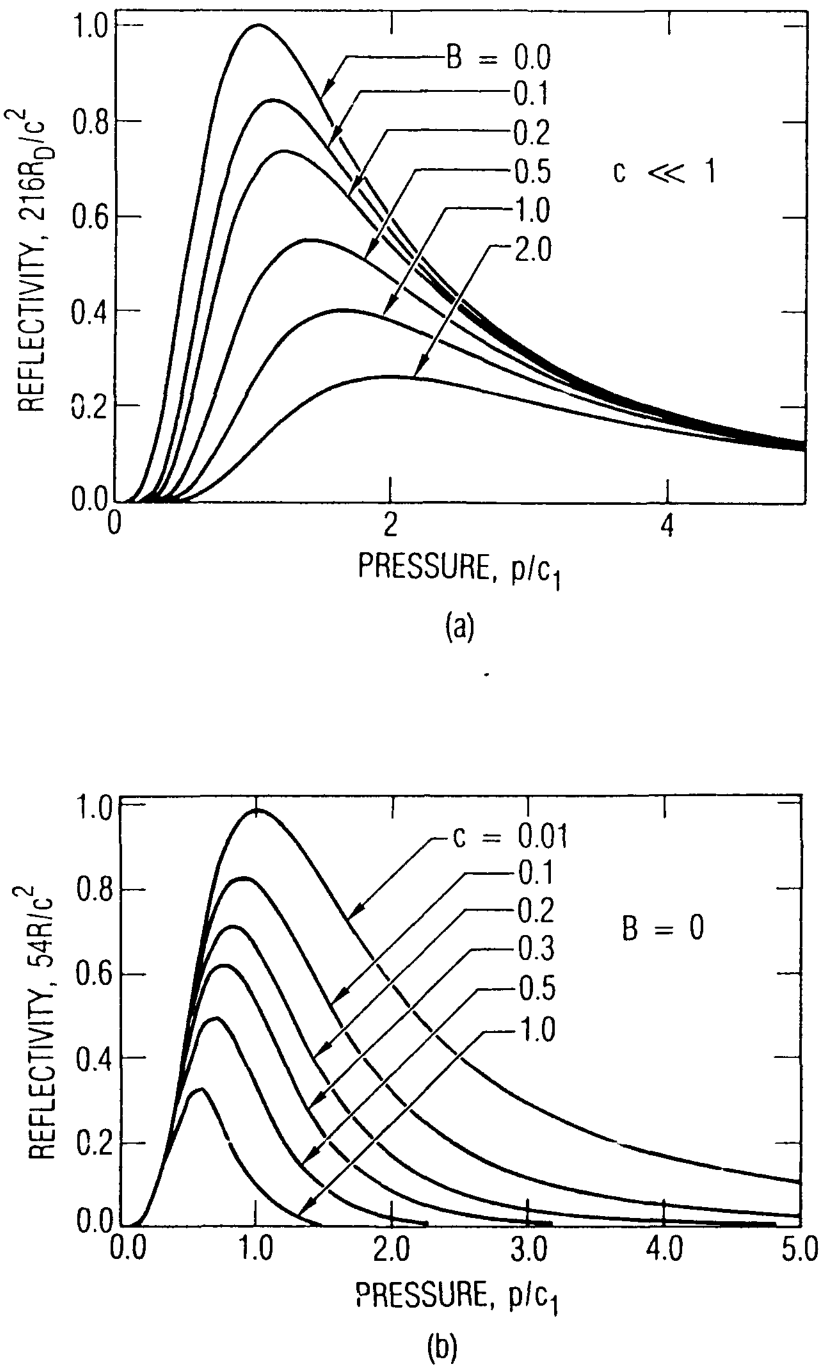

Fig. 5. Variation of Line Center Reflectivity with Pressure. (a) Effect of diffusion for case where narrow grating is fully washed out and c << 1, Eq. (9). (b) Effect of pump depletion for case where diffusion effects are negligible. The degree of pump depletion is characterized by the value of the parameter c. Appendix C.

Table 2. Maxima Associated with Variation of Reflectivity with Pressure for Inhomogeneously Broadened Medium and $I_f(0) = I_b(L)$, $I_{p,c} << I_{f,b}$, $\delta^2 << 1$, $\delta^2 << 1$.

(a) Effect of Diffusion Assuming Negligible Pump Depletion ($c<<1$) and Complete Narrow Grating Washout ($\tau Dk^2_{pb} >> 1$). See Eqs. (9) and (10) and Fig. 5a.

B	$\frac{p_m}{c_1}$	$\frac{216(R_D)_{m,p}}{c^2}$	$(\tau Dk^2_{pf})_m$
0.000	1.000	1.000	0.000
0.100	1.122	0.844	0.079
0.200	1.213	0.739	0.136
0.300	1.289	0.662	0.181
0.400	1.355	0.602	0.218
0.500	1.414	0.553	0.250
0.600	1.468	0.512	0.278
0.700	1.519	0.478	0.303
0.800	1.566	0.448	0.326
0.900	1.611	0.423	0.347
1.000	1.653	0.400	0.366
2.000	2.000	0.263	0.500
3.000	2.272	0.198	0.581
4.000	2.505	0.159	0.637
5.000	2.713	0.133	0.679
6.000	2.902	0.115	0.712
7.000	3.079	0.101	0.739
8.000	3.244	0.090	0.760
9.000	3.400	0.081	0.779
10.000	3.548	0.074	0.794

(b) Effect of Pump Depletion Assuming Negligible Diffusion. See Appendix C and Fig. 5b.

c	$\frac{p_m}{c_1}$	$\frac{54R_{m,p}}{c^2}$
0.000	1.000	1.000
0.010	0.985	0.980
0.100	0.878	0.830
0.200	0.799	0.711
0.300	0.742	0.623
0.500	0.662	0.497
0.600	0.632	0.451
1.000	0.547	0.325
3.000	0.380	0.121

In this limit

$$c = [216(R_D)_{m,p}]^{1/2} \tag{12a}$$

$$c_1 = p_m \tag{12b}$$

$$k_\alpha = [216\ (R_D)_{m,p}]^{1/2}/(p_m L) \tag{12c}$$

$$k_s = 4I_t/p_m^2 \tag{12d}$$

D. PUMP DEPLETION

In the previous sections it was assumed that the pump beam intensity did not vary along the optical path. This assumption is consistent with the assumption $\alpha_0^E L << 1$. With increase in $\alpha_0^E L$, pump depletion, due to absorption, must be considered. A computation procedure which incorporates pump depletion is outlined in Appendix C. The variation of reflectivity with pressure, at fixed-incident pump beam intensity, is indicated in Fig. 5b. Diffusion and detuning effects are neglected. The magnitude of the pump depletion effect is characterized by the parameter c, which is related to $\alpha_0^E L$. Pump depletion is seen to reduce $54R_{m,p}/c^2$ and p_m/c_1. These maxima are tabulated versus c in Table 2b.

E. GAUSSIAN PROFILE

It has been assumed that each of the beams participating in the DFWM process has a uniform intensity profile. We now assume that each beam has a Gaussian profile with a beam waist w. Reflectivity is estimated. We assume a homogeneously broadened medium and neglect diffusion and detuning.

The Gaussian profiles are expressed

$$\frac{I_c}{I_{c,0}} = \frac{I_p}{I_{p,0}} = \frac{I_t}{I_{t,0}} = e^{-2\ (r/w)^2} \tag{13}$$

where r is the transverse radius, and subscript zero denotes the centerline value. Let $P_t \equiv P_f + P_b$ denote the net pump beam power. The latter is related to $I_{t,0}$ by

$$\frac{P_t}{\pi w^2} = \frac{I_{t,0}}{2} \tag{14a}$$

$$\equiv \bar{I}_t \tag{14b}$$

Equation (14b) defines an average net pump intensity denoted $\bar{I}_t$. We now assume that the grating wavelengths λ_{pf} and λ_{pb} are small compared with w. The DFWM process at each radius r may then be assumed to be the same as that for corresponding uniform beams. The average reflection coefficient $\bar{R}$ is then

$$\bar{R} \equiv \frac{P_c}{P_p} = \frac{\int_0^\infty R I_p r \, dr}{\int_0^\infty I_p r \, dr} \tag{15}$$

which can be evaluated using Eq. (1) and Eq. (13). For $\delta^2 << 1$, the result can be expressed in the forms

$$\frac{\bar{R}}{(\alpha_0^E L)^2} = \frac{1}{16\beta} \left[\ell n(1 + 4\beta) - \frac{4\beta(1+6\beta)}{(1+4\beta)^2}\right] \tag{16a}$$

$$\frac{\bar{R}}{c^2} = \frac{1}{64\beta^2} \left[\ell n(1+4\beta) - \frac{4\beta(1+6\beta)}{(1+4\beta)^2}\right] \tag{16b}$$

where

$$\beta \equiv \frac{\bar{I}_t}{I_s} \equiv \frac{c_1^2}{4p^2} \tag{16c}$$

Equation (16a) gives the variation of $\bar{R}$ with $\bar{I}_t$ at constant p, while Eq. (16b) gives the variation of $\bar{R}$ with p at constant $\bar{I}_t$. These may be compared with the corresponding expressions for a uniform intensity profile, namely

$$\frac{R}{(\alpha_0^E L)^2} = \frac{\beta^2}{(1 + 2\beta)^3} \tag{17a}$$

and

$$\frac{R}{c^2} = \frac{1}{4}\frac{\beta}{(1 + 2\beta)^3} \tag{17b}$$

where $\beta = I_t/I_s$. Equations (16) and (17) are plotted in Fig. 6. Equations (16a) and (16b) have maxima at

$$\frac{27\bar{R}_{m,I}}{(\alpha_0^E L)^2} = 0.8278 \tag{18a}$$

$$\bar{I}_t/I_s = 1.106 \tag{18b}$$

and

$$\frac{54\bar{R}_{m,p}}{c^2} = 0.9412 \tag{19a}$$

$$p_m/c_1 = 1.147 \tag{19b}$$

The right-hand sides of Eqs. (18) and (19) equal 1 for the corresponding case of a uniform profile. Thus, the difference between the uniform and Gaussian beam is relatively small (i.e., of the order of 10 to 20% in the vicinity of the maximum reflectivity point), provided $\bar{I}_t$ is evaluated in accord with Eq. (14). The symbols R_D and $\bar{R}_D$ are used interchangeably in subsequent sections.

F. THERMAL GRATING

Thermal gratings are discussed in Appendix E. It is concluded that thermal grating effects are negligible in the present study. However, the increase in mean temperature along the optical axis, due to energy absorption, affects mean fluid properties such as k_α and k_s (e.g., Table 1) and thereby affects reflectivity.

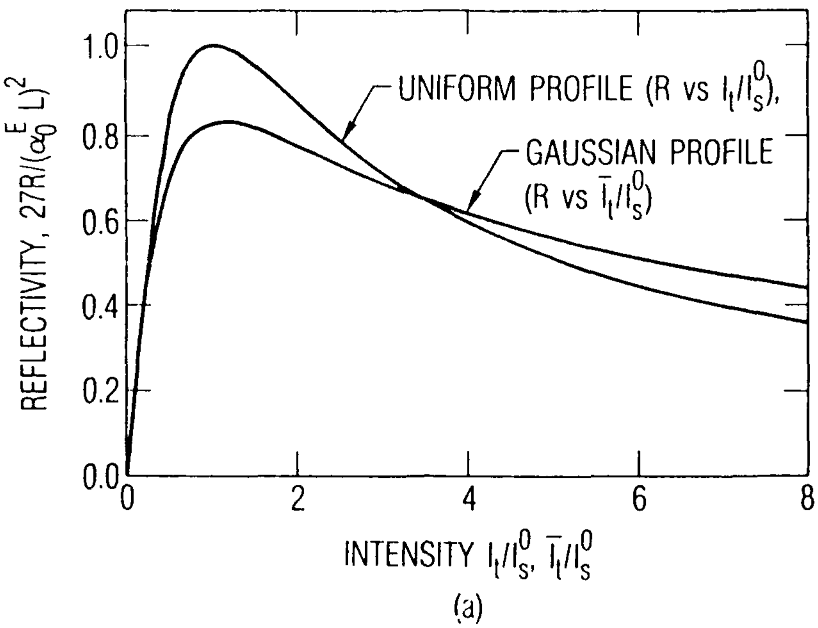

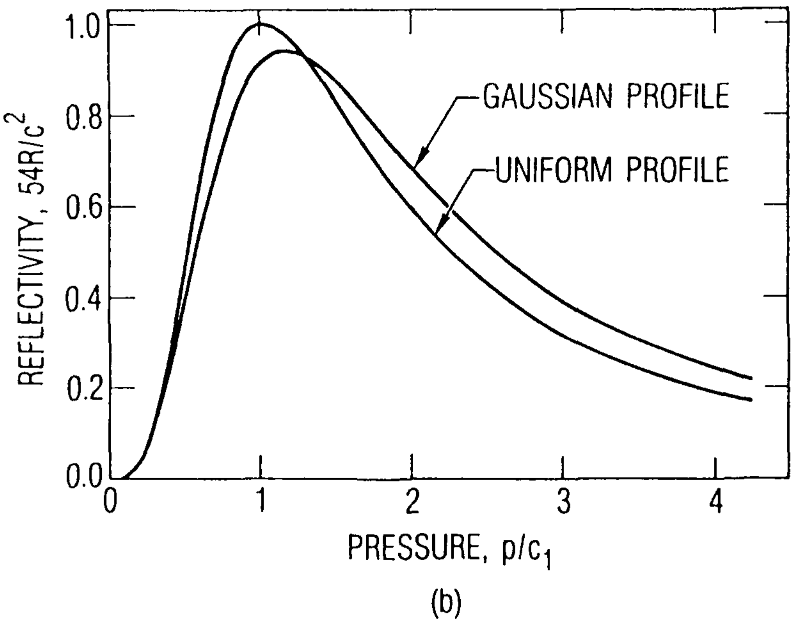

Fig. 6. Comparison of Line Center Reflectivities Associated with Uniform and with Gaussian Beam Profiles in Limit $\alpha_0^E L \ll 1$. (a) Reflectivity versus intensity. (b) Reflectivity versus pressure.

III. EXPERIMENTAL APPARATUS AND PROCEDURE

A diagram of the apparatus used in the present experiment is shown in Fig. 7. A low-power single-line cw HF laser provided two counter-propagating pump beams and an off-axis probe beam within a 10-cm-long HF absorption cell. The HF laser had a stable cavity which produced a TEM_{00} Gaussian beam in a single longitudinal mode. Power levels up to about 10 W were obtained on $P_1(8)$, $P_1(9)$, and $P_1(10)$ transitions. The Gaussian beam was focused with a concave mirror (M1) such that the forward pump beam, the backward pump beam, and the probe beam were all simultaneously focused in the center of the absorption cell. The interaction distance for the three beams was greater than the 10-cm absorption cell length. The angle between the probe beam and the forward pump was approximately 1 deg to provide good overlap of the beams and avoid washout of the wide grating. The Gaussian beam waist (radius) in the cell was 0.55 mm. The phase conjugate return signal was measured with detector D1, a LN_2-cooled HgCdTe detector.

The concave mirror of the HF laser stable-resonator was mounted on a piezoelectric-driven translation stage (Burleigh Inch Worm) so that the laser frequency for each $P_1(J)$ transition could be adjusted by varying the cavity length. During the phase conjugation reflectivity measurements, the frequency of the laser was continuously varied over a 300-MHz range using the Inch Worm driver. The 300-MHz range corresponds to the free spectral range of the resonator cavity and is approximately equal to the Doppler width of the HF absorption line at 300 K. Laser frequency was monitored with a scanning confocal interferometer using the 1% reflected beam from beamsplitter BS 0.

A chopper was used on the probe beam so that a lock-in amplifier could discriminate the small reflected-conjugate signal from scattered cw light and other noise sources. Beam blocks were inserted in the optical path of the probe and pump beams to verify that the observed signal was produced by the interaction of all three beams within the absorbing HF medium. A removable retroreflector and some removable neutral-density filters were

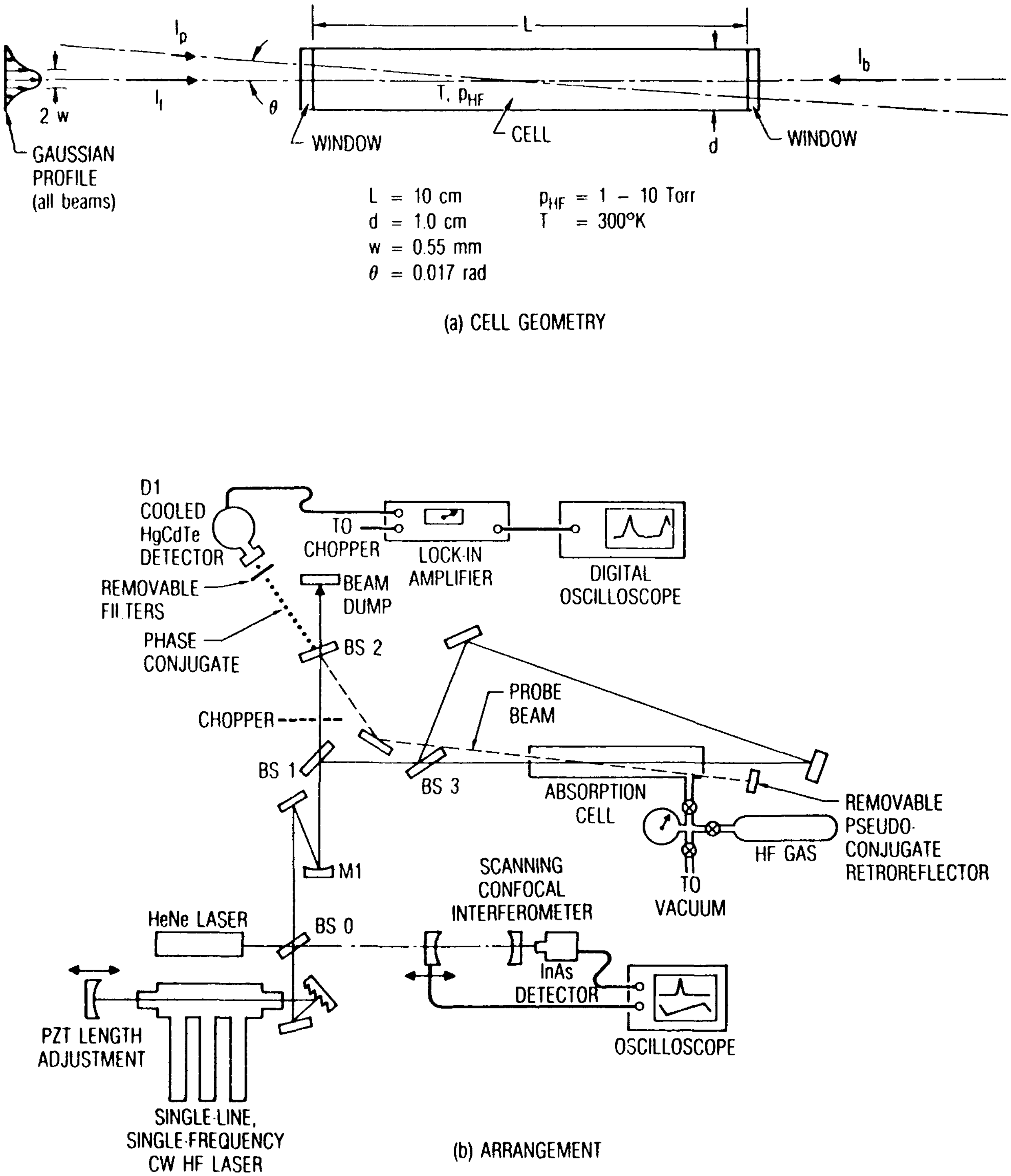

Fig. 7. Experimental Apparatus. (a) Cell geometry, (b) Arrangement.

used to position the detector at the location of the conjugate return beam, to calibrate the reflectivity measurement, and to establish reflected signal-to-noise ratio. Signal-to-noise ratios as high as 60 were measured. The ratio of reflected signal on line-center to background off line-center was usually about 5 to 1. In most cases, the difference between these two signals was used to evaluate the reflected signal when calculating conjugate reflectivity.

IV. EXPERIMENTAL RESULTS

A. DETUNING EFFECT

The variation of conjugate intensity with detuning $\nu-\nu_0$ is indicated in Fig. 8. For the present case, the Doppler and homogeneous widths are $\Delta\nu_d \approx 300 \times 10^6$ Hz and $\Delta\nu_h \approx 30 \times 10^6$ Hz, respectively. It is seen that the FWHM (full width at half maximum) of the conjugate signal is of the order of $\Delta\nu_h$. This is expected from physical reasoning because only particles within the frequency range $\Delta\nu_h$ about line center are resonant with the three input beams I_f, I_b, and I_p. These results also support the present use of a homogeneous theory (with appropriate absorption and saturation coefficients) to model DFWM in an inhomogeneously broadened medium.

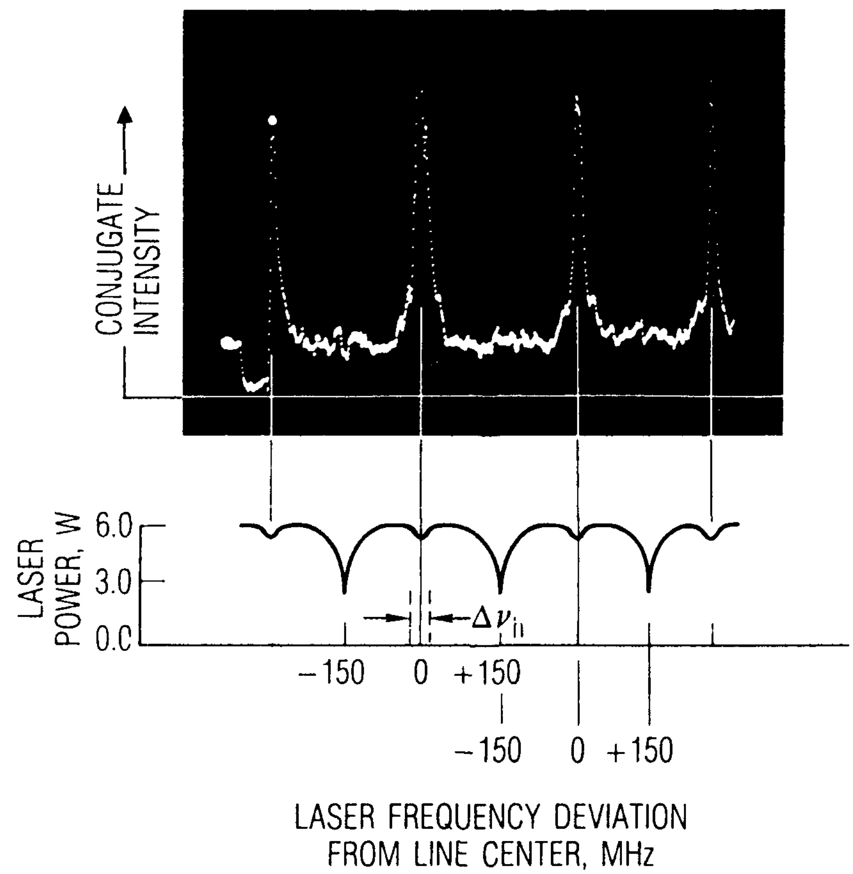

Fig. 8. Effect of Detuning on Conjugate Signal Intensity.

B. PRESSURE VARIATION EFFECT

The variation of line center ($\delta = 0$) reflection coefficient R_D with pressure p is given in Fig. 9 for three transitions $P_1(8)$, $P_1(9)$, and $P_1(10)$ with pump intensities $\bar{I}_t$ = 130, 600, and 400 W/cm^2, respectively. The maximum reflectivity $(R_D)_{m,p}$ is of the order of 10^{-4} and occurs at pressures p_m from 2 to 4 Torr. The experimental values of $(R_D)_{m,p}$ and p_m, deduced from Figs. 9a to 9c, are listed in Table 3c.

Figures 9 include theoretical estimates for the variation of R_D with p. These were obtained using Eq. (9a) with an analytical estimate for B and with arbitrary choices for c and c_1. The latter were chosen so that the experimental and theoretical curves were in agreement at the maximum point. The shapes of the theoretical and experimental curves are in approximate agreement.

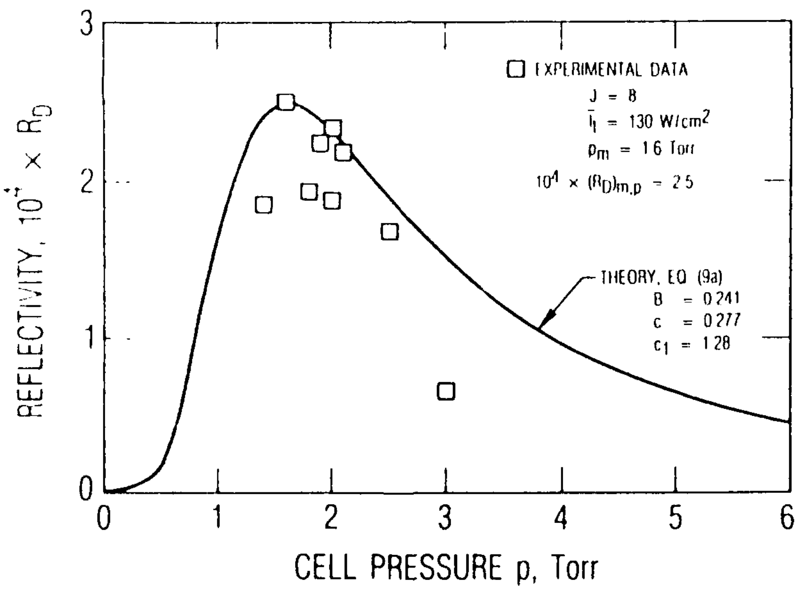

(a)

Fig. 9. Variation of Line Center Reflectivity with Cell Pressure for Fixed Average Intensity $\bar{I}_t$. Experimental data denoted by squares. Theoretical curves are based on Eq. (9a) using values of c and c_1 chosen to match experimental values of $(R_D)_{m,p}$ and p_m. (a) Transition $P_1(8)$, intensity $\bar{I}_t$ = 130 W/cm^2. (b) Transition $P_1(9)$, intensity $\bar{I}_t$ = 600 W/cm^2. (c) Transition $P_1(10)$, intensity $\bar{I}_t$ = 400 W/cm^2.

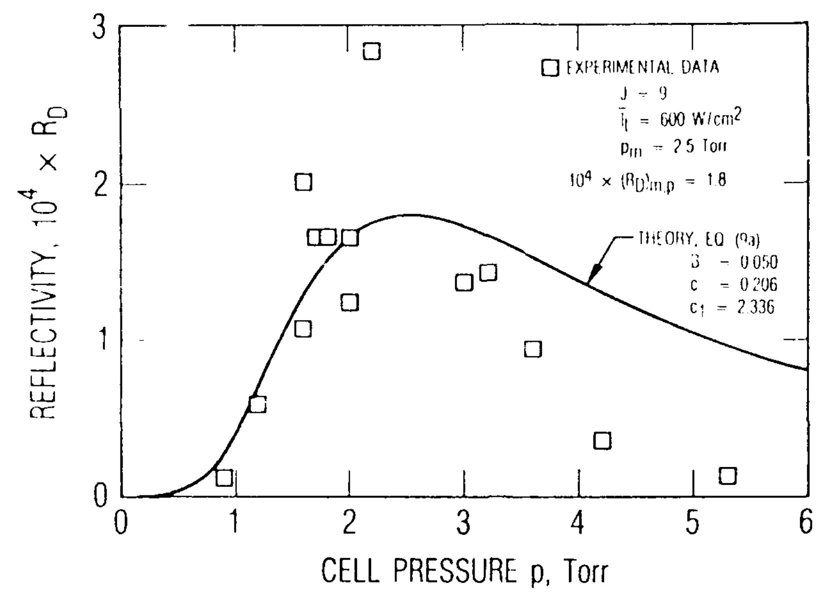

(b)

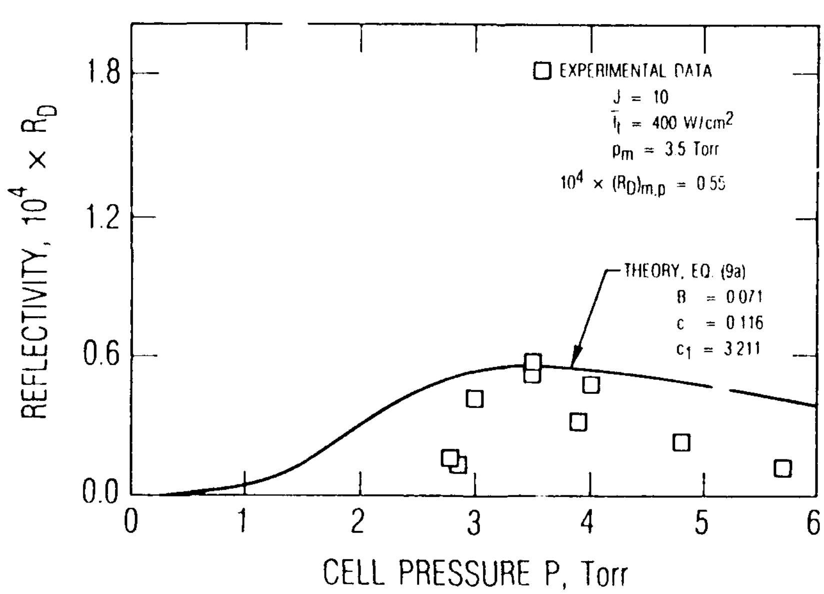

(c)

Fig. 9 (concluded)

Table 3 represents an attempt to compute $(R_D)_{m,p}$ and p_m from purely analytical considerations. Table 3a contains estimates for k_α, k_s, c, c_1 and B. The latter are based on a temperature T = 300 K and thereby neglect laser heating. The estimates for $(R_D)_{m,p}$ and p_m in Table 3a are based on Eq. (9a) and take diffusion into account. Table 3b corrects these estimates for Gaussian profile and pump depletion effects. The corrected theory in Table 3b agrees with the experiment to within a factor of about 2, except for the value of $(R_D)_{m,p}$ for the case J = 10. The poor agreement for this case is probably due to the present neglect of the induced temperature rise. (Note, from Table 1, that the variation of k_α with T is greatest for the J = 10 case.)

Thermocouple measurements near the optical axis indicate temperature increases of the order 50-100 K due to absorption of laser radiation. The latter measurements were made by R. M. Kurtz. Further study is needed of the magnitude of the temperature rise and its effect on reflectivity.

Table 3. Comparison of Theory and Experiment for p_m and $(R_D)_{m,p}$

(a) Theory for Case of Uniform Profile and Negligible Pump Depletion (T = 300 K, θ = 0.017 rad, L = 10 cm). (Eq. 9a).

Theory										
J	$\bar{I}_t$ (W/cm^2)	κ_α (Table 1)	k_s (Table 1)	c_1 $[2(I_t/k_s)^{1/2}]$	c $(k_\alpha L\, c_1)$	B $(1.68/c_1^2)$	p_m/c_1 (Table 2a)	$\frac{216(R_D)_{m,p}}{c^2}$ (Table 2a)	p_m (Torr)	$(R_d)_{m,p}$ $(\times 10^4)$
8	130	0.01897	74.60	2.64	0.501	0.241	1.25	0.705	3.30	8.19
9	600	0.00364	71.14	5.81	0.211	0.050	1.07	0.913	6.22	1.88
10	400	0.00056	68.03	4.85	0.0272	0.071	1.09	0.882	5.29	0.030

(b) Corrections to Theory

	Correction Factors: Gaussian Profile (Eq. 19)		Correction Factors: Pump Depletion (Table 2b)		Corrected Theory	
J	$\frac{p_m}{c_1}$	$\frac{54R_{m,p}}{c^2}$	$\frac{p_m}{c_1}$	$\frac{54R_{m,p}}{c^2}$	p_m (Torr)	$(R_D)_{m,p}$ $(\times 10^4)$
8	1.15	0.94	0.66	0.50	2.50	3.85
9	1.15	0.94	0.79	0.70	5.65	1.24
10	1.15	0.94	0.96	0.95	5.84	0.03

(c) Experiment

p_m (Torr)	$(R_D)_{m,p}$ $(\times 10^4)$
1.6	2.5
2.5	1.8
3.5	0.55

V. CONCLUDING REMARKS

The present study may be viewed as a first attempt to investigate phase conjugation of a cw HF laser beam by use of an HF absorption cell. Emphasis has been placed on the variation of reflectivity with pressure. The theoretical development included consideration of diffusion, thermal conduction, pump depletion and Gaussian profile effects. Further study is needed, particularly with regard to temperature effects and conjugation fidelity.

REFERENCES

1. Duignan, M. T., Feldman, B. J., Gibson, N. D., and Whitney, W. T., "Stimulated Brillouin Scattering of Multiline Hydrogen Fluoride Laser Radiation," SPIE Vol 874, 1988, p. 25.

2. Koop, C. G., "Stimulated Brillouin Scattering at 2.9 μm," International Conference on Lasers '88, Harvey's Resort Hotel, Lake Tahoe, Nevada, December 4-9, 1988.

3. Shen, Y. R., The Principles of Nonlinear Optics, John Wiley & Sons, 1984, pp. 187-192.

4. Abrams, R. L. et al., "Phase Conjugation and High-Resolution Spectroscopy by Resonant Degenerate Four-Wave Mixing," in R. A. Fisher, Optical Phase Conjugation, Academic Press, 1983, pp. 211-284.

5. Reintjes, J. F., Nonlinear Optical Parametric Processes in Liquids and Gases, Academic Press, 1984, pp. 377-392.

6. Brown, W. P., "Absorption and Depletion Effects on Degenerate Four-Wave Mixing in Inhomogeneously Broadened Absorbers," J. Opt. Soc. Am., Vol. 73, No. 5, May 1983, pp. 629-634.

7. Gruneisen, M. T., Gaeta, A. L., and Boyd, R. W., "Exact Theory of Pump-Wave Propagation and its Effect on Degenerate Four-Wave Mixing in Saturable-Absorbing Media," J. Opt. Soc. Am. B, Vol. 2, No. 7, July 1985, pp. 1117-1121.

8. Galushkin, M. G., Nikitin V. Yu, and Oraevskii, A. N., "Phase Conjugation of an Optical Wave in the Case of Degenerate Four-Wave Interaction in an Amplifying Medium of a Chemical HF Laser," Sov. J. Quantum Electron. 18 (1), January 1988, p. 87.

9. Mirels, H., "Inhomogeneous Broadening Effects in cw Chemical Lasers," AIAA J., Vol. 17, No. 5, May 1979, p. 478.

10. Mirels, H., "Effects of Translational and Rotational Nonequilibrium on cw Chemical Laser Performance," Appl. Opt., Vol. 27, No. 1, 1 January 1988, p. 89.

11. Svehla, R. A., "Estimated Viscosities and Thermal Conductivities of Gases at High Temperatures," NASA Technical Report, R-132, 1962.

12. Zel'dovich, B. Ya., Pilipetsky, N. F., and Shkunov, V.V., "Principles of Phase Conjugation," Springer-Verlag, Berlin, 1985, pp. 176-184.

13. Caro, R. G., and Gower, M. C., "Phase Conjugation by Degenerate Four Wave Mixing in Absorbing Media," IEEE J. Quantum Electron., Vol. QE-18, No. 9, September 1987, p. 1376.

APPENDIX A

SYMBOLS

B	parameter characterizing diffusion effect, Eq. (9b)
c	$k_\alpha L c_1$
c_1	$2(I_t/k_s)^{1/2}$
D	diffusion coefficient Eq. (D-1)
k	wave number of incident waves
k_{ij}	wave number associated with $\varepsilon_i + \varepsilon_j$ waves
k_α	absorption coefficient parameter, Eq. (7a)
k_s	saturation intensity parameter, Eq. (7b)
I	intensity
I_t	sum of pump wave intensities, $I_f + I_b$
I_s, I_s^0	saturation intensity, Eq. (2b)
L	length of cell
$P_1(J)$	P-branch transition from $v = 0$, J to $v = 1$, $J-1$
P_t	net power in Gaussian profile pump waves, $P_f + P_b$
p	cell pressure
r	transverse radius
R	reflection coefficient in absence of diffusion, I_c/I_p
R_D	reflection coefficient in presence of diffusion, I_c/I_p
$(R_D)_{m,p}$	reflectivity maximum associated with pressure variation, Eq. (11)
T	temperature
w	Gaussian profile beam waist, Eq. (13)
α	electric field absorption coefficient at low power
α_0^E	line center value of α
δ	detuning, $(\nu-\nu_0)/(\Delta\nu_h/2)$
$\bar{\varepsilon}_i$	ith electric field, Eq. (C-2a)
θ	angle between I_p and I_f
λ	wavelength of incident waves
λ_{ij}	wavelength associated with ε_i and ε_j waves
ν	frequency of incident waves, s^{-1}

ν_0	line center frequency of resonant absorber
$\Delta\nu_d$	Doppler width (FWHM)
$\Delta\nu_h$	homogeneous width (FWHM) of resonant absorber, Eq. (B-2)

Subscripts

τ	lifetime of upper level
ω	frequency of incident waves, rad/s
δ	detuning parameter, Eq. (2c)
f,b,p,c	refers to forward pump, backward pump, probe,and conjugate waves, respectively.
i	refers to ith wave
j	refers to jth wave
ij	refers to combination of ith and jth waves
m	associated with maximum point

Superscript

$(\bar{\ })$	vector quantity or average value

APPENDIX B
MOLECULAR DATA FOR HF

Notation: Dimensions used herein are p_{HF} (Torr), T(K), λ(cm), α_0^E (cm^{-1}), $\nu(s^{-1})$, $k_\alpha(cm^{-1} Torr^{-1})$, $k_s(W\ cm^{-2}\ Torr^{-2})$, $I_s^0(W\ cm^{-2})$

Doppler Width (FWHM):

$$\Delta\nu_d = \frac{8.316 \times 10^4}{\lambda} \left(\frac{T}{300}\right)^{1/2} \tag{B-1}$$

where λ is in centimeters.

Homogeneous Width (FWHM):

$$\Delta\nu_h = 1.5 \times 10^7 \left(\frac{300}{T}\right)^{1/2} p_{HF} \tag{B-2}$$

Equation (B-2) is based on a mean value for HF-HF collisions.[9]

Absorption Coefficient:[9]

$$\alpha_0^E = \frac{2.13 \times 10^{11}}{T^{3/2}} \frac{(1 + v - 0.01v^3)(1 + 0.063J)J}{\exp[J(J + 1)T_R/T]} \times \left[n_v - n_{v+1}e^{2JT_R/T}\right] \tag{B-3a}$$

where T_R = 30.16 K for HF. Equation (B-3a) assumes an inhomogeneously broadened medium in the limit $\Delta\nu_h/\Delta\nu_d << 1$ and applies for laser P-branch transitions

$$v, J \rightleftarrows v + 1, J-1 \tag{B-3b}$$

where v,J denote the vibrational and rotational energy level of the absorbing particle. An alternate notation for the P-branch transition is $P_{v+1}(J)$. The quantities n_v and n_{v+1} denote number density, in moles/cm^3, of particles in the lower and upper vibrational level, respectively. At room temperature, under nonlasing conditions, $n_{v+1}/n_v << 1$ and Eq. (B-3a) becomes

$$k_\alpha \equiv \frac{\alpha_0^E}{p_{HF}} = \frac{3.42 \times 10^6}{T^{5/2}} \frac{(1 + v - 0.01v^3)(1 + 0.063J)J}{\exp[J(J + 1)T_R/T]} \tag{B-3c}$$

where the equation of state $n_v = 1.603 \times 10^{-5}\, p_{HF}/T$ has been used. Values of k_α are listed in Table 1.

Wavelength for $P_1(J)$ Transition:

$$10^4\lambda = 2.7441;\ 2.7826;\ 2.8231;\ 2.8657 \tag{B-4}$$

$$J = 7;\ 8;\ 9;\ 10$$

Saturation Intensity:

A definition of saturation intensity, consistent with Eq. (D-1), is

$$I_s^0 = \frac{1}{\tau(\bar{\sigma}/\varepsilon)_{v,J}} \equiv k_s p_{HF}^2 \tag{B-5a}$$

where I_s^0 is line center saturation intensity, τ is mean particle collision time (i.e., upper level lifetime), and

$$\left(\frac{\bar{\sigma}}{\varepsilon}\right)_{v,J} = \frac{3.79 \times 10^{13}}{\pi^2 \Delta\nu_h} \frac{J(1 + 0.063J)(1 + v - 0.01v^3)}{(2J + 1)} \quad \frac{cm^2}{J} \tag{B-5b}$$

is the cross section for photon absorption.[10] Substitution into Eq. (B-5a) indicates, by use of Eq. (B-11),

$$k_s = 52.79 \frac{(2J + 1)\ (300/T)^{1.4}}{J(1 + 0.063J)(1 + v - 0.01v^3)} \tag{B-5c}$$

Values of k_s are listed in Table 1.

Gas Properties:

Density

$$\rho = 1.069 \times 10^{-6}\ p_{HF}(300/T) \quad g/cm^3 \tag{B-6}$$

Index of refraction

$$n - 1 = 5.0 \times 10^{-7}\ P_{HF}(300/T) \tag{B-7a}$$

$$\frac{\Delta n}{\Delta T} = (-1)\ 1.7 \times 10^{-9}\ P_{HF}(300/T)^2 \tag{B-7b}$$

Specific heats

$$c_p = 1.46 \qquad J/(g\text{-}K) \tag{B-8a}$$

$$\gamma = c_p/c_v = 1.4 \tag{B-8b}$$

Mean particle spread $\bar{v}$ and sound speed a

$$\bar{v} = [8/(\gamma\pi)]^{1/2}a = \lambda\Delta\nu_d(\pi \ln 2)^{-1/2} \tag{B-9a}$$

$$= 5.64 \times 10^4\ (T/300)^{1/2} \qquad cm/s \tag{B-9b}$$

Mean free path

$$\ell = \frac{\mu}{0.499\,\rho\bar{v}} = \frac{4.17 \times 10^{-3}}{p_{HF}} \left(\frac{T}{300}\right)^{1.4} \quad \text{cm} \tag{B-10}$$

Mean collision time

$$\tau = \frac{\ell}{\bar{v}} = \frac{7.40 \times 10^{-8}}{p_{HF}} \left(\frac{T}{300}\right)^{0.9} \quad \text{s} \tag{B-11}$$

Comparison of Eqs. (B-2) and (B-11) indicates $\pi\Delta\nu_h\tau = 3.5$. The latter expression equals 1 for a simple billiard ball model.

Transport properties:[11]

Viscosity

$$\mu = 1.25 \times 10^{-4} \left(\frac{T}{300}\right)^{0.9} \quad \frac{\text{g}}{\text{cm-s}} \tag{B-12}$$

Thermal conductivity

$$k_T = 2.64 \times 10^{-4} \left(\frac{T}{300}\right)^{0.9} \quad \frac{\text{J}}{\text{cm-s-K}} \tag{B-13}$$

Diffusion coefficient

$$D = \frac{1.33\mu}{\rho} = 1.56 \times 10^{2} \frac{(T/300)^{1.9}}{p_{HF}} \quad \frac{\text{cm}^2}{\text{s}} \tag{B-14}$$

Grating washout parameter for $\theta^2 \ll 1$,

$$\tau D k_{pf}^2 = \frac{1.68}{p_{HF}^2} \left(\frac{T}{300}\right)^{2.8} \left(\frac{\theta}{0.017} \frac{2.8 \times 10^{-4}}{\lambda}\right)^2 \tag{B-15}$$

APPENDIX C
DEGENERATE FOUR-WAVE MIXING THEORY

Expressions are derived that define reflection coefficients associated with four-wave mixing in a homogeneously broadened medium. The configuration of Fig. 1 is assumed with $\theta^2 << 1$ and $I_{p,c} << I_{f,b}$. Pump depletion effects are included.

The electric susceptibility of a homogeneously broadened medium is

$$\chi = -\frac{2i(1 - i\delta)}{k} \frac{\alpha}{1 + (I/I_s)} \tag{C-1a}$$

where

$$\delta = (\nu - \nu_0)/[\Delta\nu_h/2] \tag{C-1b}$$

$$\alpha = \alpha_0^E/(1 + \delta^2) \tag{C-1c}$$

$$I_s = I_s^0(1 + \delta^2) \tag{C-1d}$$

Here α_0^E is the low-power electric-field absorption coefficient evaluated at line center, I_s is saturation intensity, and I_s^0 is the line center saturation intensity [e.g., Eq. (B-5a)]. Other symbols are defined in Appendix A.

Components of the electric field are expressed in the form

$$\bar{\varepsilon}_i = \frac{1}{2}[E_i e^{i\omega t} + c.c.] \tag{C-2a}$$

where

$$E_i/E_s \equiv A_i(z)e^{-i\bar{k}_i \cdot \bar{z}} \tag{C-2b}$$

and $E_s \equiv (2I_s/\varepsilon c)^{1/2}$ is the electric field associated with the saturation intensity I_s. The net local intensity I is then

$$\frac{I}{I_s} \equiv \left|\frac{E}{E_s}\right|^2 = \frac{1}{2} \sum_i \sum_j A_i A_j^* e^{-i\bar{k}_{ij} \cdot \bar{z}} \tag{C-3a}$$

where

$$\bar{k}_{ij} \equiv \bar{k}_i - \bar{k}_j \tag{C-3b}$$

$$|\bar{k}_{ij}| \equiv k_{ij} = 2\pi/\lambda_{ij} \tag{C-3c}$$

Here i and j each take on the values f, b, p, and c. For $i \neq j$, Eq. (C-3) defines interference terms. The wavelengths of the wide and narrow gratings in Fig. 2 are then, respectively,

$$\frac{\lambda_{pf}}{\lambda} \equiv \frac{k}{k_{pf}} = \frac{1}{2 \sin (\theta/2)} \tag{C-4a}$$

$$\frac{\lambda_{pb}}{\lambda} \equiv \frac{k}{k_{pb}} = \frac{1}{2 \cos (\theta/2)} \tag{C-4b}$$

Substitution of Eqs. (C-1a) and (C-3a) into the electromagnetic wave equation yields,[4-7] for $E_{p,c} << E_{f,b}$,

$$\frac{dA_f}{dz} = - \alpha_f A_f \tag{C-5a}$$

$$\frac{dA_b}{dz} = \alpha_b A_b \tag{C-5b}$$

$$\frac{dA_p}{dz} = - \alpha_p A_p + \kappa A_c^* \tag{C-5c}$$

$$\frac{dA_c}{dz} = \alpha_p A_c - \kappa A_p^* \tag{C-5d}$$

where

$$\alpha_{f,b} = \alpha(1-i\delta)\left[\frac{1}{q} + \frac{1}{2A_{f,b}^2}\left(1 - \frac{1 + A_f^2 + A_b^2}{q}\right)\right]$$

$$\alpha_p = \alpha(1 - i\delta)\left(\frac{1 + A_f^2 + A_b^2}{q^3}\right) \equiv \alpha_{pR} + \alpha_{pI}$$

$$\kappa = \alpha(1 - i\delta)\left(\frac{2A_fA_b}{q^3}\right)$$

$$q = \left[1 + 2(A_f^2 + A_b^2) + (A_f^2 - A_b^2)^2\right]^{1/2}$$

$$A_i^2 = |A_i|^2 = I_i/I_s$$

The boundary conditions at z = 0 and z = L are

$$A_f(0) = \text{GIVEN} \qquad A_p(0) = \text{GIVEN} \tag{C-6a}$$

$$A_b(L) = \text{GIVEN} \qquad A_c(L) = 0 \tag{C-6b}$$

Equations (C-5c) and (C-5d) can be combined to yield an expression for the ratio $r(z) \equiv A_c/A_p^*$, namely,

$$\frac{dr}{dz} = 2\alpha_{pR}r - \kappa - \kappa^* r^2 \tag{C-7a}$$

$$r(L) = 0 \tag{C-7b}$$

where r(0) defines the reflection coefficient. Equation (C-7) is now integrated for the cases of zero and nonzero pump depletion.

(a) Zero Pump Depletion ($\alpha L << 1$)

If pump depletion effects are neglected, the coefficients in Eq. (7a) are independent of z and Eq. (7a) can be integrated to yield

$$R \equiv |r(0)|^2 = \left|\frac{\kappa}{\alpha_{pR} + w \cot wL}\right|^2 \tag{C-8a}$$

where

$$w = \sqrt{|\kappa|^2 - \alpha_{pR}^2} \tag{C-8b}$$

Note that $R \equiv I_c(0)/I_p(0)$ is the intensity reflection coefficient for the four-wave mixing process. In the limit $\alpha L << 1$, which is consistent with the neglect of pump depletion, Eq. (8a) becomes

$$R = |\kappa L|^2 \,[1 + \mathbf{O}(\alpha_{pR}L)] \tag{C-9a}$$

or, equivalently,

$$(1 + \delta^2)\,\frac{R}{(\alpha_0^E L)^2} = \frac{(I_t/I_s)^2\,(1 - d^2)\,[1 + \mathbf{O}(\alpha_{pR}L)]}{[1 + 2(I_t/I_s) + (I_t/I_s)^2 d^2]^3} \tag{C-9b}$$

where $I_t = I_f + I_b$, and $d = |I_f - I_b|/I_t$. The case $d = 0$, $\alpha_{pR}L \sim \alpha_0^E L$ is considered in Eq. (1).

(b) Nonzero Pump Depletion [$\alpha L = \mathbf{O}(1)$]

In the case of nonzero pump depletion, it is convenient to write Eqs. (C-5a) and (C-5b) in the form

$$\frac{d(I_f/I_s)}{dz} = -\,2\alpha_{fR}\,\frac{I_f}{I_s} \tag{C-10a}$$

$$\frac{d(I_b/I_s)}{dz} = 2\alpha_{bR}\frac{I_b}{I_s} \qquad \text{(C-10b)}$$

where

$$I_f(0)/I_s = \text{GIVEN} \qquad \text{(C-10c)}$$

$$I_b(L)/I_s = \text{GIVEN} \qquad \text{(C-10d)}$$

Here α_{fR} and α_{bR} are the real parts of α_f and α_b, respectively. The reflectivity r(0) is found by integrating Eqs. (C-7) and (C-10) in the interval $0 \leq z \leq L$. The latter is a two-point boundary value problem which can be reduced to a one-point boundary value problem by evaluating $I_f(L)/I_s$ analytically and integrating from z = L to z = 0. When $I_f(0) = I_b(L)$, the analytic solution for $I_f(L)/I_s$ is found from (e.g., Ref. 7)

$$D + \frac{D}{|D|}\ln\frac{|D| + [D^2 + 2(1 + K)]^{1/2}}{[2(1 + K)]^{1/2}} = \alpha L \qquad \text{(C-11)}$$

where

$$K = S - (D^2 + 2S + 1)^{1/2}$$

$$S = [I_b(L) + I_f(L)]/I_s$$

$$D = [I_b(L) - I_f(L)]/I_s$$

Equation (C-11) applies for gain as well as absorption. Numerical results for the variation of R with pressure, for a fixed pump intensity, are given in Fig. 5b. Pump depletion effects increase with increase in the parameter c, which is related to $\alpha_0^E L$. Maxima, from Fig. 5b, are listed in Table 2b.

APPENDIX D
DIFFUSION EFFECT

Particle diffusion reduces the effectiveness of the gratings induced by the four-wave mixing process.[12] The diffusion effect is estimated herein.

We first consider a homogeneously broadened medium. Let n_1 and n_2 denote particle number density in the lower and upper laser energy levels. For weak saturation, $n_2 \ll n_1$, the variation of n_2 with time is given by

$$\frac{\partial n_2}{\partial t} = - \frac{n_2}{\tau} + \frac{n_1}{\tau} \left|\frac{E}{E_s}\right|^2 + D\nabla^2 n_2 \tag{D-1}$$

where τ is n_2 particle lifetime and D is the diffusion coefficient. For the case of multiple electric fields given by Eq. (C-3a), the steady state solution of Eq. (D-1) is

$$\frac{n_2}{n_1} = \frac{1}{2} \sum_i \sum_j \frac{A_i A_j^*}{1 + \tau D k_{ij}^2} e^{-i\bar{k}_{ij}\cdot\bar{z}} \tag{D-2}$$

Each term in Eq. (D-2), for $i \neq j$, corresponds to an interference grating. The effect of diffusion is to reduce the amplitude of each grating by the factor $(1 + \tau D k_{ij}^2)^{-1}$. The reflectivity coefficient R given in Eq. (C-8a) is the result of two gratings with amplitudes proportional to $A_f A_p^*$ and $A_b A_p^*$, respectively. Let R and R_D denote estimates of reflectivity which exclude and include the effect of diffusion, respectively. It follows that

$$\frac{R_D}{R} = \left(\frac{1/2}{1 + \tau D k_{pf}^2} + \frac{1/2}{1 + \tau D k_{pb}^2}\right)^2 \tag{D-3}$$

where the terms involving k_{pf} and k_{pb} correspond to the wide and narrow gratings, respectively, in Fig. 2.

Equations (D-1) and (D-3) apply to an inhomogeneously broadened medium for cases where $\delta < 1$ (i.e., for cases where the laser radiation interacts with particles which have low thermal velocity.) In these cases, τ is the mean particle collision time. It can be shown from expressions in Appendix B that $\tau Dk^2 \sim (\Delta\nu_d/\Delta\nu_h)^2$. It follows that

$$\tau Dk_{pf}^2 \sim \left(\frac{\Delta\nu_d}{\Delta\nu_h}\right)^2 \left(2 \sin \frac{\theta}{2}\right)^2 \tag{D-4a}$$

$$\tau Dk_{pb}^2 \sim \left(\frac{\Delta\nu_d}{\Delta\nu_h}\right)^2 \left(2 \cos \frac{\theta}{2}\right)^2 \tag{D-4b}$$

For an inhomogeneously broadened medium, $\Delta\nu_h << \nu_d$, the narrow grating is always washed out (i.e., $\tau Dk_{pb}^2 >> 1$). The wide grating will be fully effective (i.e., $\tau Dk_{pf}^2 << 1$) when

$$(\theta\Delta\nu_d/\Delta\nu_h)^2 << 1 \tag{D-5}$$

In the latter case, the right-hand side of Eq. (D-3) is equal to 1/4. Equation (D-5) indicates the need for small θ when $\Delta\nu_d/\Delta\nu_h$ is large.

APPENDIX E
THERMAL GRATING

In the present experiment, laser energy continuously heats the absorbing medium. After an initial transient, an elevated steady-state temperature distribution is established along the optical axis. This steady state temperature has an average value such that heat loss by radial conduction and by convection equals the energy input. The increase in average temperature, due to laser heating, appears to be of the order of 100 K in the present experiments. In addition, there are small periodic variations in temperature associated with each of the standing waves established by the four-wave mixing process. The corresponding refractive index variations constitute thermal gratings which are similar to the saturation-induced gratings discussed in Appendix C. The reflectivity associated with the thermal gratings is deduced herein.

The net heat addition per unit volume, per unit time, due to laser radiation, is given by

$$2\alpha I \equiv \alpha I_s \sum_i \sum_j A_i A_j^* e^{-i\vec{k}_{ij} \cdot \vec{z}} \tag{E-1}$$

The equation for conservation of energy becomes

$$\alpha I_s \sum_i \sum_j A_i A_j^* e^{-i\vec{k}_{ij} \cdot \vec{z}} = \rho c_p \frac{\partial T}{\partial t} + q - k_T \nabla^2 T \tag{E-2}$$

where q is the local energy loss per unit volume, per unit time, due to radial conduction and convection, and k_T is the thermal conductivity coefficient. Under steady state conditions, the solution of Eq. (E-2) is, for $i = j$,

$$q = \alpha I_s \sum_i A_i^2 = 2\alpha \sum_i I_i \tag{E-3a}$$

and for $i \neq j$

$$\Delta T_{ij} = \frac{\alpha I_s}{k_T} \frac{A_i A_j^*}{k_{ij}^2} e^{-i\bar{k}_{ij} \cdot \bar{z}} \tag{E-3b}$$

The average temperature along the optical axis is the value for which radial conduction and convection permit Eq. (E-3a) to be satisfied. The quantity ΔT_{ij} in Eq. (E-3b) is the temperature perturbation associated with the grating defined by $\bar{k}_{ij}$.

Denote the local index of refraction by $n = n_0 + \Delta n$ where Δn denotes the perturbation due to ΔT. The electric susceptibility is then

$$\begin{aligned} \chi &= n^2 - 1 \\ &= (n_0^2 - 1) + 2n_0 \frac{\Delta n}{\Delta T} \sum_i \sum_j \Delta T_{ij} \end{aligned} \tag{E-4}$$

Substitution into the wave equation yields

$$\frac{dA_p}{dz} = \kappa A_c^* \tag{E-5a}$$

$$\frac{dA_c}{dz} = -\kappa A_p^* \tag{E-5b}$$

where

$$\kappa = \frac{2ik\alpha}{k_T k_{pf}^2} \frac{\Delta n}{\Delta T} (I_f I_b)^{1/2} \left(1 + \frac{k_{pf}^2}{k_{pb}^2}\right) \tag{E-5c}$$

Note that $k_{pf}^2/k_{pb}^2 = \tan^2(\theta/2)$ so that this term (i.e., contribution of the narrow grating) can be neglected in Eq. (E-5c). Comparison with Eqs. (C-5) and (C-8) indicates that the reflectivity associated with the thermal grating is

$$R_{th} = \tan^2|\kappa|L \tag{E-6}$$

Thermal gratings induced by a pulsed laser, with pulse length τ and negligible conduction, have been investigated.[13] The present results agree with those in Ref. 13 if $(k_T k_{pb}^2)^{-1}$ is replaced by $\tau/\rho c_p$ in Eq. (E-5c). This equivalence can be deduced directly from Eq. (E-2).

Evaluation of Eq. (E-6) for typical conditions of the present experiment indicates $R_{th} \sim 10^{-10}$. The reflectivity associated with saturation is of order $R \sim 10^{-4}$. Hence, thermal gratings play no role in the present experiment. However, the increase in mean temperature along the optical axis does affect fluid property values and thereby affects the performance of the saturation gratings.

LABORATORY OPERATIONS

The Aerospace Corporation functions as an "architect-engineer" for national security projects, specializing in advanced military space systems. Providing research support, the corporation's Laboratory Operations conducts experimental and theoretical investigations that focus on the application of scientific and technical advances to such systems. Vital to the success of these investigations is the technical staff's wide-ranging expertise and its ability to stay current with new developments. This expertise is enhanced by a research program aimed at dealing with the many problems associated with rapidly evolving space systems. Contributing their capabilities to the research effort are these individual laboratories:

Aerophysics Laboratory: Launch vehicle and reentry fluid mechanics, heat transfer and flight dynamics; chemical and electric propulsion, propellant chemistry, chemical dynamics, environmental chemistry, trace detection; spacecraft structural mechanics, contamination, thermal and structural control; high temperature thermomechanics, gas kinetics and radiation; cw and pulsed chemical and excimer laser development, including chemical kinetics, spectroscopy, optical resonators, beam control, atmospheric propagation, laser effects and countermeasures.

Chemistry and Physics Laboratory: Atmospheric chemical reactions, atmospheric optics, light scattering, state-specific chemical reactions and radiative signatures of missile plumes, sensor out-of-field-of-view rejection, applied laser spectroscopy, laser chemistry, laser optoelectronics, solar cell physics, battery electrochemistry, space vacuum and radiation effects on materials, lubrication and surface phenomena, thermionic emission, photosensitive materials and detectors, atomic frequency standards, and environmental chemistry.

Electronics Research Laboratory: Microelectronics, solid-state device physics, compound semiconductors, radiation hardening; electro-optics, quantum electronics, solid-state lasers, optical propagation and communications; microwave semiconductor devices, microwave/millimeter wave measurements, diagnostics and radiometry, microwave/millimeter wave thermionic devices; atomic time and frequency standards; antennas, rf systems, electromagnetic propagation phenomena, space communication systems.

Materials Sciences Laboratory: Development of new materials: metals, alloys, ceramics, polymers and their composites, and new forms of carbon; nondestructive evaluation, component failure analysis and reliability; fracture mechanics and stress corrosion; analysis and evaluation of materials at cryogenic and elevated temperatures as well as in space and enemy-induced environments.

Space Sciences Laboratory: Magnetospheric, auroral and cosmic ray physics, wave-particle interactions, magnetospheric plasma waves; atmospheric and ionospheric physics, density and composition of the upper atmosphere, remote sensing using atmospheric radiation; solar physics, infrared astronomy, infrared signature analysis; effects of solar activity, magnetic storms and nuclear explosions on the earth's atmosphere, ionosphere and magnetosphere; effects of electromagnetic and particulate radiations on space systems; space instrumentation.